PERGAMON

European Journal of Cancer 38 (2002) 2147–2156

European Journal of Cancer

www.ejconline.com

Magnetic resonance imaging in cancer research

B.D. Ross[a,b,*], T.L. Chenevert[a], A. Rehemtulla[c]

[a]*Department of Radiology, University of Michigan Medical School, 1150 West Medical Center Drive, Medical Sciences Research Building III, Room 9303, Ann Arbor, MI 48109-0648, USA*

[b]*Department of Biological Chemistry, University of Michigan Medical School, 1150 West Medical Center Drive, Medical Sciences Research Building III, Room 9303, Ann Arbor, MI 48109-0648, USA*

[c]*Department of Radiation Oncology, University of Michigan Medical School, 1150 West Medical Center Drive, Medical Sciences Research Building III, Room 9303, Ann Arbor, MI 48109-0648, USA*

Received 14 February 2002; accepted 21 February 2002

Abstract

Non-invasive assessment of antineoplastic response and correlation of the location, magnitude and duration of transgene expression *in vivo* would be particularly useful for evaluating cancer gene therapy protocols. This review presents selected examples of how magnetic resonance (MR) has been used to assess therapeutic efficacy by non-invasive quantitation of cell kill, to detect a therapeutic response prior to a change in tumour volume and to detect spatial heterogeneity of the tumour response and quantitate transgene expression. In addition, applications of the use of bioluminescence imaging (BLI) for the evaluation of treatment efficacy and *in vivo* transgene expression are also presented. These examples provide an overview of areas in which imaging of animal tumour models can contribute towards improving the evaluation of experimental therapeutic agents.

Keywords: MRI; Yeast cytosine deaminase; Bioluminescence imaging (BLI); Molecular imaging; Glioma; Cancer gene therapy

1. Introduction

The use of *in vitro* screening assays to quantitate the effectiveness of anticancer agents are widely used to rapidly evaluate a wide variety of agents and doses. Drugs which show therapeutic promise are then evaluated against animal tumour models. For orthotopic tumour models, animal survival, colony-forming efficiency (CFE) assays of cells disaggregated from solid tumours, and measurements of excised tumour weights have been used to quantitate efficacy [1] since serial measurements of tumour growth rates are difficult to obtain. The myriad of new antineoplastic agents on the horizon requiring *in vivo* testing underscores the need for improved high-throughput surrogate markers for preclinical evaluation of therapeutic efficacy. The application of non-invasive imaging methods for quantitating the effects of experimental treatments could accelerate the process of drug development for translation to clinical trials [2].

The use of imaging for cancer patients has become an essential aspect of clinical care. However, the significant advances in molecular biology along with the imaging sciences have provided additional unique opportunities for interrelated applications between these two research areas. In fact, the dramatic advances in imaging and biology has led the National Cancer Institute (NCI) in the United States to identify cancer imaging as an "Extraordinary Opportunity" for funding [3]. The combination of molecular biology and the imaging sciences has melded into a new research field termed 'molecular imaging' which crosses into all imaging modalities used in cancer including magnetic resonance imaging (MRI) [4–18], radionuclide imaging [19–27], X-ray computed tomography (CT) [28,29] and optical imaging methods [30–42]. This review will cover examples of recent work using MRI to assess therapeutic efficacy by non-invasive quantitation of cell kill, early detection of therapeutic response, detection of spatial heterogeneity of tumour response and quantitation of transgene expression. Examples of the use of bioluminescence

* Corresponding author. Tel.: +1-734-763-2099; fax: +1-734-647-2563.

E-mail address: bdross@umich.edu (B.D. Ross).

0959-8049/02/$ - see front matter © 2002 Elsevier Science Ltd. All rights reserved.
PII: S0959-8049(02)00387-8

imaging (BLI) for *in vivo* evaluation of treatment and for detection of transgene expression are also presented. The successful application of these imaging technologies to assess experimental interventions of *in vivo* tumour models can provide unique insights related to therapeutic efficacy.

2. Quantitation of tumour cell kill using MRI and BLI

Measurements of orthotopic tumour volumes in individual animals over time is not possible without the use of imaging technologies, hence the majority of studies quantitate therapeutic response using statistical evaluation of animal survival times. This approach has proved valuable for *in vivo* testing of therapeutic approaches, but requires large numbers of animals due to variations in tumour growth kinetics between animals. MRI has been recently reported [2] for non-invasively monitoring the growth kinetics and therapeutic response of the intracranial rat 9L brain tumour model [1]. Shown in Fig. 1 are representative series of T2-weighted MR images of a rat with a 9L brain tumour acquired pre- and posttreatment with the chemotherapeutic agent 1,3-bis(2-chloroethyl)-1-nitrosourea (BCNU). The tumour is revealed as a hyperintense mass in the right hemisphere which, following treatment, shrinks in size before regrowing at a later time. These multislice MR data sets acquired over time allow for quantitation of tumour volume which can be plotted to yield the growth kinetics (tumour doubling time) and response to therapy in an individual animal as shown in Fig. 1. This approach allows for quantitation of tumour cell kill in individual animals [2]. In brief, $\log(\text{cell kill}) = \log_{10}(V_{\text{pre}}/V_{\text{post}})$ where V represents the tumour volume obtained from MRI measurements before (pre) and following (post) therapeutic intervention. As each animal serves as their own pretreatment control, the use of MRI provides for a very sensitive approach (quantitation of >0.1 log kill can be detected). The use of MRI is applicable to a wide variety of therapeutic interventions and tumour models for facilitating evaluation of experimental interventions.

Application of optical-based methods for *in vivo* tumour detection and evaluation of treatments is an active area of research. Fluorescence and bioluminescence optical imaging approaches for cancer detection and monitoring treatment are very promising. The use of BLI necessitates detection of light emitted from expression of the bioluminescent enzyme firefly luciferase (Luc) from tumour cells [10,39]. We have recently shown BLI can provide data which allows for the quantification of therapeutic efficacy of orthotopic 9L brain tumours in rats [10]. Expression of Luc in 9L tumour cells ($9L^{luc}$) was accomplished. Implantation of $9L^{luc}$ cells into rats resulted in tumours which could be visualised by MRI as well as BLI. Shown in Fig. 2

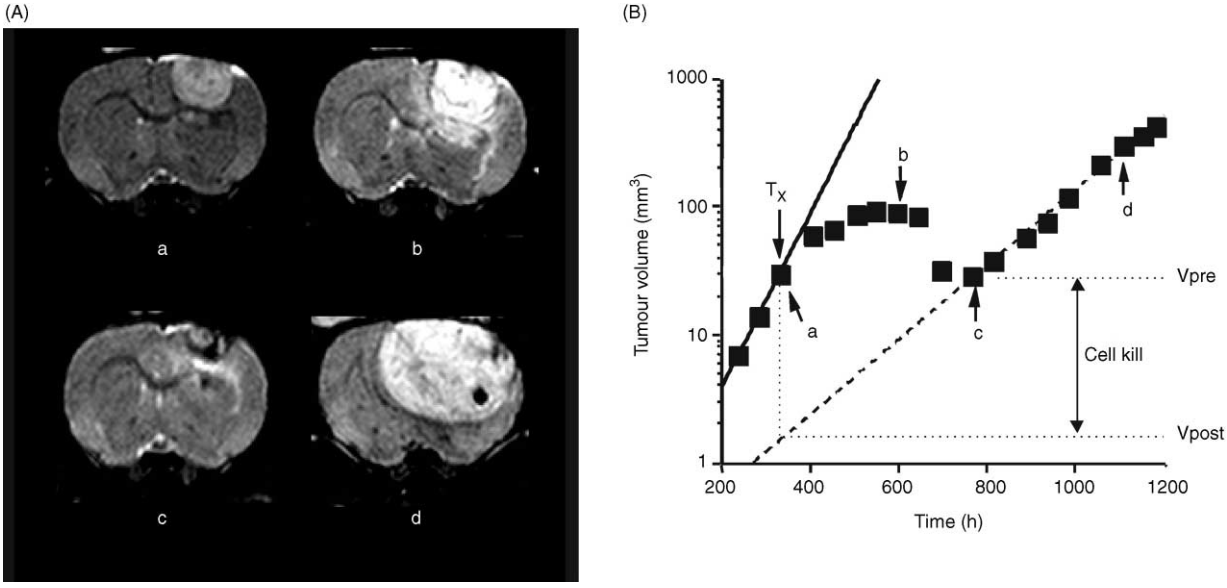

Fig. 1. A series of coronal T_2-weighted MR images of a rat harbouring a 9L tumour in the right hemisphere (A) within 2 h following 1,3-bis(2-chloroethyl)-1-nitrosourea (BCNU) treatment ($2\times LD_{10}$). Each displayed image is from approximately the same region of the brain. (B) Tumour volumes obtained from serial MR images of the rat are displayed versus time following 9L cell implantation with the time intervals depicted by the arrows corresponding to the tumour MR images (a)–(d). In each case, the individual volume measurements are shown along with the line corresponding to the least-squares fit. Individual volume measurements are shown along with the pretreatment (solid) and posttreatment (dashed) lines corresponding to the least-squares fit of exponential growth curves following treatment with $2\times LD_{10}$ BCNU. Pre- and post-BCNU doubling times (T_d) were 46 and 99 h, respectively, revealing a decrease in growth rate during post treatment exponential tumour re-growth. The calculated log cell kill value was 1.6. The arrows denoted by (a)–(d) correspond with the rat brain MR images shown in (a) and correspond to the postcell implantation time points of 330, 593, 763 and 1105 h, respectively.

(upper left panel) are a series of MR images (top) with the corresponding optical images (bottom) acquired over time in an animal treated with BCNU. A quantitative plot of the MRI volumetric data and the BLI photon counts over time is also shown in Fig. 2 (right panel). This data was used to calculate the log(cell kill) as described above. Comparison of log kill values using these two imaging techniques revealed similar results (Fig. 2 lower panel) [10].

BLI offers a relatively rapid quantification of tumour size (tumour volume is proportional to photon count [10]), however, it is currently limited to a single two-dimensional image with limited spatial resolution. MRI provides a three-dimensional tomographic image set which provides the investigator with additional information such as the heterogeneity and spatial extent of the tumour mass. This is especially important for transplanted tumour models where transplanted cells may not all grow in the precise, localised site of injection. For example, implantation of brain tumour cells into brain parenchyma may also produce extracerebral extension of the tumour mass above the site of injection. This feature would not be distinguishable using BLI, but could be easily discerned using MRI. Another potential issue related to BLI is that there is the possibility of the luciferase protein expressed by the transplanted cell eliciting an immune response, a well-known phenomenon with other optical reporters such as green fluorescent protein (GFP). As the brain is considered to be an immune privileged site, this may not be a significant concern for neuro-oncology studies, but must be considered for other organ sites. The decision of which imaging modality to use will depend upon the type of data required for a particular study.

3. Diffusion MRI

The clinical value of conventional MRI stems from the ability to non-invasively observe the gross tumour morphology and follow changes over time and/or treatment. There remains large untapped potential for using MR technology to provide significant functional, structural and molecular information. Such information may be derived from quantitation of tissue properties which reflect, for example, perfusion dynamics, oxygenation levels, biochemistry/metabolism, cellularity and levels of gene expression.

One very interesting application of MRI is its use to follow therapeutic-induced macroscopic changes in tumours. Since molecular and cellular changes typically precede observable macroscopic changes in gross

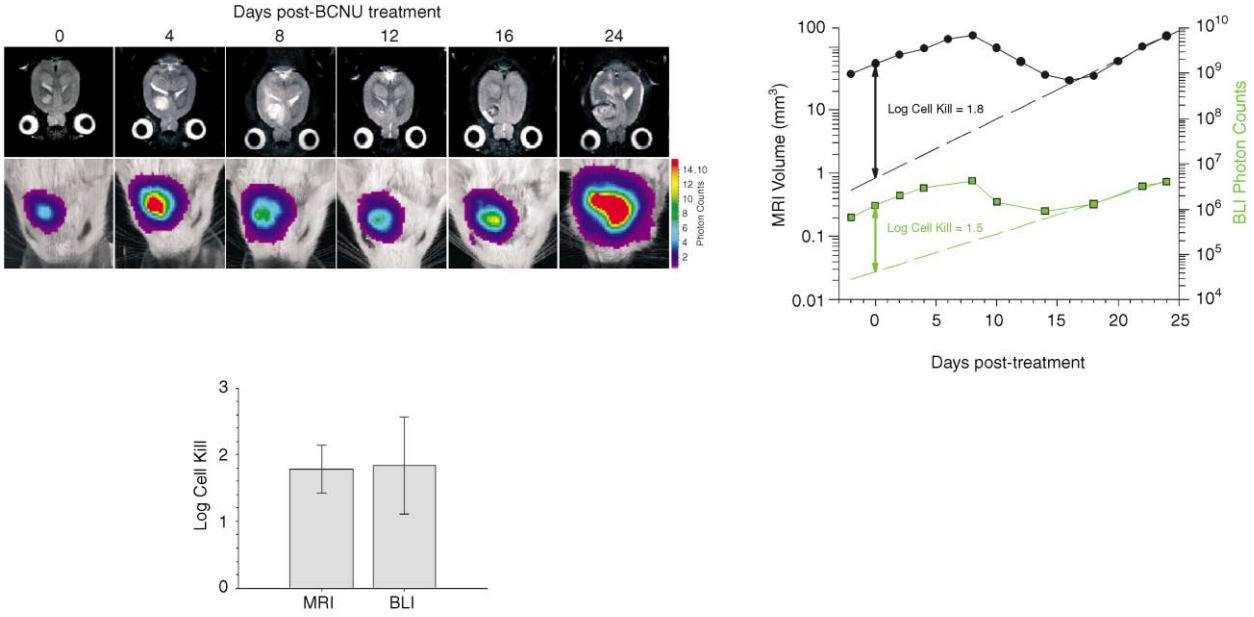

Fig. 2. Temporal analysis of the response of a $9L^{Luc}$ tumour to BCNU chemotherapy. Tumour cells were implanted 16 days prior to treatment. Tumour volume was monitored with T_2-weighted MRI (left panel, top row) and intratumoral luciferase activity was monitored with BLI (left panel, bottom row). The days post-BCNU therapy on which the images were obtained are indicated at the top. The scale to the right of the BL images describes the colour map for the photon count. Quantitative analysis of tumour progression and response to BCNU chemotherapy is shown in the top right panel. Tumour volumes (●) and total tumour photon emission (■) obtained by T_2-weighted MRI and BLI, respectively, are plotted versus days post-BCNU treatment. The dashed lines are the regression fits of the exponential tumour repopulation following therapy. The solid vertical lines denote the apparent tumour-volume and photon-production losses elicited by BCNU on the day of treatment from which log cell kill values were calculated. Comparison of log cell kill values determined from MRI and BLI measurements is shown in the bottom panel. Log cell kill elicited by BCNU chemotherapy was calculated using MRI (1.78 ± 0.36) and BLI (1.84 ± 0.73). Data are represented as mean ± standard error of the mean (SEM) for each animal ($n = 5$). There was no significantly significant difference between the log kills calculated using the MRI and BLI data ($P = 0.951$).

tumour size, the use of MRI to quantitate therapeutic-induced changes in tumour cellularity using a surrogate marker (i.e. water diffusion) has been recently reported [7]. The use of water diffusion as a surrogate marker to probe tissue is compelling since this parameter is strongly affected by viscosity and membrane permeability between intra- and extracellular compartments, active transport and flow, and directionality of tissue/cellular structures that impede or enhance mobility. As depicted in Fig. 3 (top panel), successful treatment of tumours can result in significant damage and/or killing of cells thus altering cell membrane integrity. This has a net effect of increasing the fractional volume of the interstitial space due to apoptotic body formation and cell loss resulting in an increase in the mobility (diffusion) of water within the damaged tumour tissue. Diffusibility of tissue water *in vivo* can be non-invasively quantified as an apparent diffusion coefficient (ADC) using diffusion MRI where the MR signal intensity is made dependent on water mobility by application of additional pulsed magnetic field gradients to the MR sequence [43]. Quantitation of ADC values can be obtained since individual nuclear spins of water molecules within the tumour tissue accumulate a phase shift proportional to their spatial position within the magnetic field gradient. These water molecules are then given an evolution time to diffuse followed by application of an identical, but inverse, pulse which results in a complete refocusing of stationary spins, while the mobile spins (those undergoing movement due to diffusion) are refocused incompletely. The net result is that the paired gradient pulses attenuate the signal in proportion to the local water mobility within that region of tissue. Quantitative measurements of diffusion reported as an ADC are obtained by measuring signal attenuation as a function of varying gradient strength and evolution time.

An example of the application of diffusion MRI for monitoring therapeutic-induced changes in tumour tissue is shown in Fig. 3 (bottom panel). In this figure, diffusion MRI was used to detect early changes in water diffusion values in a rat 9L brain tumour following treatment with BCNU (single dose of 26.6 mg/kg, intraperitoneally (i.p.)). ADC images are shown for a single slice acquired over several time points where the intensity of the signal is proportional to the diffusion value of the water molecules within that tissue region (voxel). Prior to chemotherapy, the signal within the tumour tissue is slightly enhanced relative to that of normal brain as evidenced by the elevated signal intensity

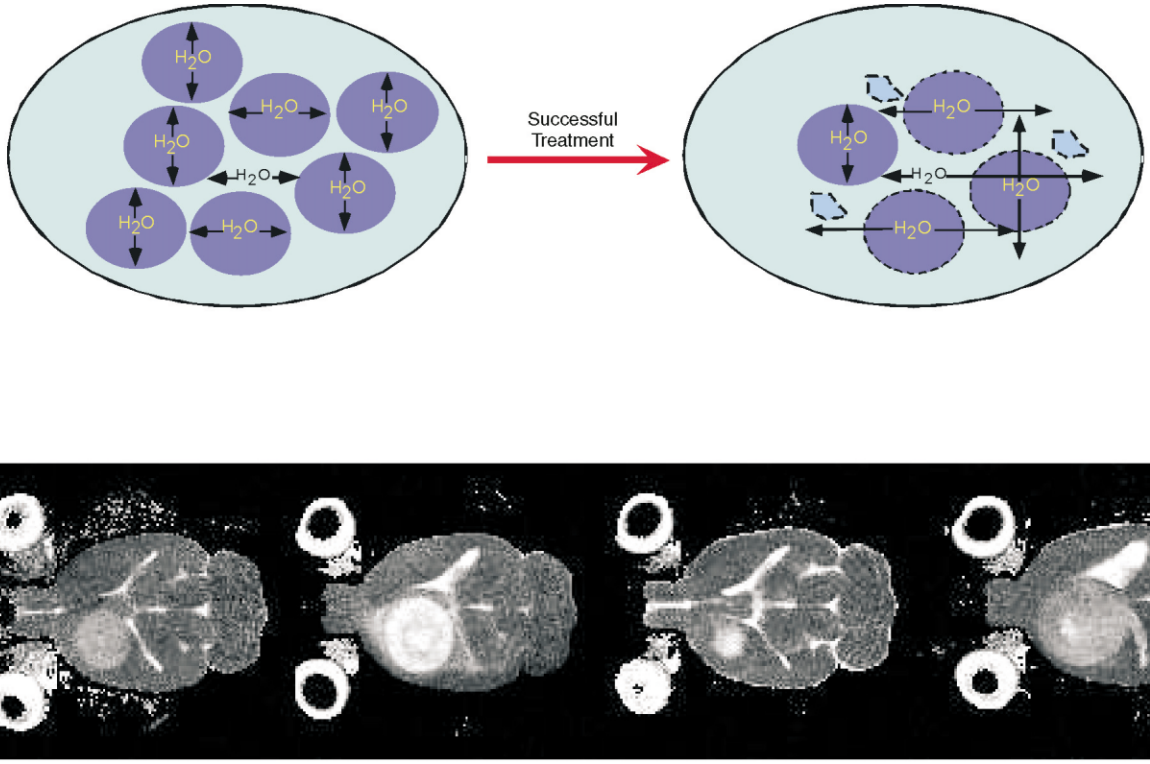

Fig. 3. Top panel: Schematic of the 'Diffusion Hypothesis'. Diffusion of water within tumour cells is limited by cell membranes. Diffusion of water in the interstitial space is also limited by the high density of tumour cells. Treatments which kill cells compromise cell membrane integrity, and may cause cells to fragment or apoptose and become smaller, thereby removing barriers to diffusion. These changes should occur before changes in overall tumour volume (ovals). Bottom panel: Apparent diffusion coefficient (ADC) maps of a rat brain with a 9L glioma on days 0, 8, 17 and 28 days following BCNU treatment (from left to right, respectively). The brighter the intensity, the more freely (faster) water is able to move (diffuse) within the tumour tissue.

within the tumour mass. Following BCNU administration, the diffusibility of water in the tumour increased significantly (second image from left), although the tumour continued to expand revealing that this technique is able to detect early events in the cell death process prior to regression of the tumour mass. The increase in water ADC values (signal intensity) was due to a significant increase in extracellular water within the tumour tissue as the density of cells decreased due to therapeutic-induced death. Removal of the cellular debris at later time points resulted in shrinkage of the primary mass followed by a return to previous diffusion values during subsequent regrowth of the tumour. The use of diffusion MRI for monitoring early events in tumour treatment in a variety of rodent tumours models [4,7,13,44–49] has been reported along with a preliminary clinical translation to patients with primary central nervous system (CNS) tumours [49]. The use of diffusion MRI has potential for monitoring early changes in tumours which may be reflective of treatment response. It is envisioned that imaging approaches such as this may assist physicians in tailoring treatments for individual patients and allow for alternative therapies to be attempted in a more timely fashion if a tumour is found to be resistant. This approach also provides the significant potential of assessing the regional/spatial heterogeneity of therapeutic response within a tumour. The heterogeneity of response may be accentuated in applications involving direct intratumoral administration of the therapeutic agent as is done in certain therapeutic protocols involving cancer gene therapy.

4. Imaging of cancer gene therapy

The goal of cancer gene therapy is to overcome the dose-limiting systemic toxicity of chemotherapy by introducing a gene into tumour cells which encodes for an enzyme that converts low-toxicity prodrugs into potent cytotoxic agents. The effectiveness of this approach depends on sufficient transgene expression and localised conversion of a prodrug to the cytotoxic compound, the relative sensitivity of the tumour to this agent and finally the ability of the cytotoxic agent to reach a majority of the tumour cells. Non-invasive assessment of therapeutic response and correlation of the location, magnitude and duration of transgene expression would be useful in facilitating optimisation of gene transfer protocols, vector development and prodrug dosing schedules.

4.1. Imaging gene therapy response

Diffusion MRI has been shown to evaluate the response of orthotopic 9L gliomas to the adenoviral delivered yeast cytosine deaminase (*yCD*) gene therapy paradigm [13,48]. The prodrug used in these studies was Flucytosine (5-fluorocytosine, 5-FC). 5-FC itself does not elicit cytotoxicity, and its efficacy depends on the ability of the microbial enzyme CD to convert 5-FC to the antimetabolite 5-fluorouracil (5-FU). yCD is not found in mammals, thus providing 5-FC with a favourable therapeutic index. As shown in Fig. 4, expression of the *yCD* gene specifically in tumour cells, followed by systemic administration of 5-FC will result in the generation of 5-FU within the tumour. This localised production of 5-FU chemotherapy avoids the systemic toxicity associated with intravenous 5-FU therapy and may improve outcomes by achieving higher intratumoral 5-FU concentrations.

yCD and other gene therapy strategies are particularly suited to treatment of CNS malignancies such as glioma since unlike other solid malignancies, gliomas rarely metastasise making local control of primary tumour burden the focus of therapy. This facilitates tumour-specific delivery/targeting of therapeutic genes by direct stereotactic injection, even when the tumour is not surgically resectable. In addition, the normal CNS parenchyma surrounding gliomas is mitotically inactive; thus the therapeutic index for proliferating cell-selective cytotoxic agents may be improved by local production of the agent within the CNS. A study was undertaken using 9L cells which had been genetically modified to express yCD in order to determine the effectiveness of this novel treatment under optimal conditions wherein

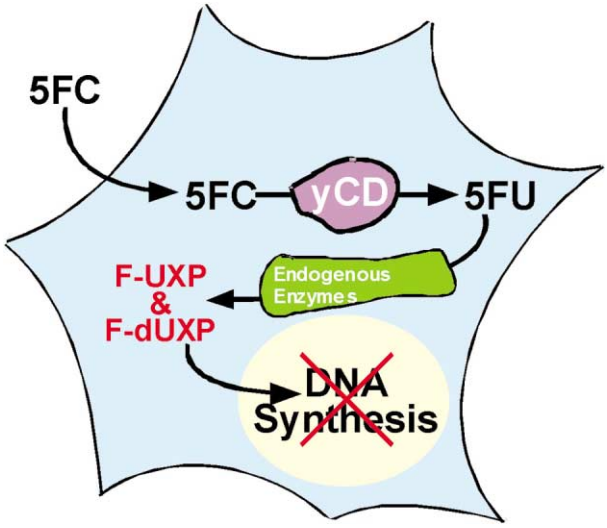

Fig. 4. Schematic of *yCD*/5-FC gene therapy. Transfer of the cDNA for CD into tumour cells causes them to express the CD protein. Upon entering such transduced tumour cells, 5-FC is converted to the chemotherapeutic agent 5-fluorouracil (5-FU). Like 5-fluorocytosine (5-FC), 5-FU is membrane permeable and may leave the transduced cell to kill neighbouring tumour cells. Endogenous enzymes form fluorinated nucleotides (FNuct) from 5-FU. FNuct's mediate the cytotoxicity of CD/5-FC gene therapy via thymidylate synthase inhibition by 5-fluoro-2′-deoxyuridine-5′-monophosphate (FdUMP), disruption of nucleotide pools, and incorporation into RNA.

each tumour cell contained the expressed transgene and also to investigate the ability of diffusion MRI to follow treatment [48]. Shown in Fig. 5a are a series of ADC maps of a rat with a 9L tumour expressing the *yCD* transgene which was treated over time with daily doses of 5-FC beginning on day 0. The signal intensity of the treated tumour began to significantly increase during the first week of treatment compared with control animals as shown in the diffusion histograms (Fig. 5b and c). These histograms contain the average total number of image pixels contained within the 9L tumours ($n = 5$/group) plotted versus ADC values with the corresponding dynamic changes in the mean ADC values shown in the inset. A significant feature of this data are that the changes in diffusion values occurred prior to shrinkage of the tumour volume indicating that this imaging approach can detect early changes in the tumour mass following initiation of gene therapy. Moreover, a symmetrical shift towards higher diffusion values for the entire tumour mass was observed which indicated that the entire tumour mass was affected by this therapy. Since this approach was found to cure intracerebral 9L tumours when cells uniformly expressed the transgene, a follow-up study was undertaken to investigate a more therapeutically relevant paradigm in which the *yCD* gene was transferred to a solid tumour using an adenoviral vector.

The effects of the heterogeneous distribution of *yCD* transgene expression on tumour cell viability was examined using diffusion-weighted MRI [13]. Shown in Fig. 6 (upper left panel) is a diffusion-weighted transverse MR image of a rat 9L tumour treated with the *yCD* adenoviral vector, but did not receive the prodrug phosphate-buffered saline ((PBS)-treated). In this image, the brightness of the tissue region (or voxels) is proportional to the diffusibility of water with the bright regions within the normal brain corresponding to cerebral spinal fluid located within the ventricular space. The tumour, located in the right hemisphere, has overall a slightly higher diffusion value than that of the normal brain parenchyma. In addition, the tumour image displays a relatively uniform pattern of diffusion values indicating a uniform (untreated or non-necrotic) distribution of cellular structures (e.g. intra- and extracellular

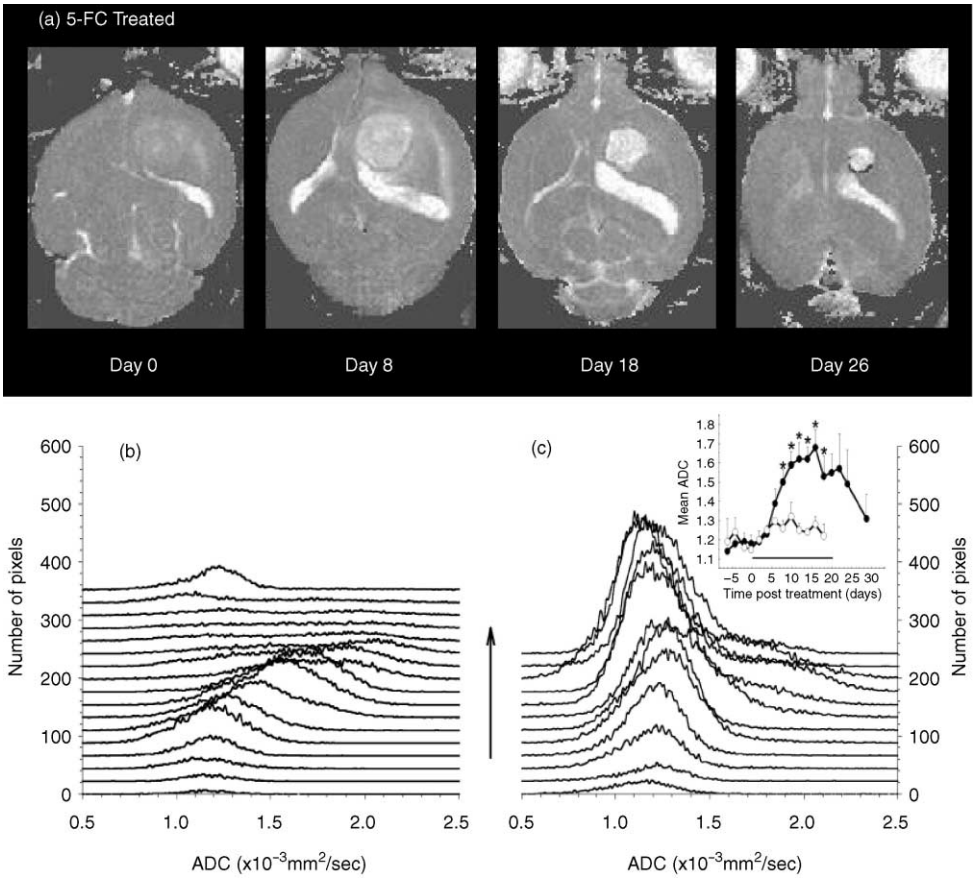

Fig. 5. (a) Isotropic ADC images during 5-fluorocytosine (5-FC) treatment of a rat harbouring an intracerebral 9L glioma expressing yCD. The times indicated are relative to the beginning of 5-FC treatment. Pixel intensity are proportional to measured ADC values. Serial histograms of ADC values for (b) 5-FC treated and (c) control tumours over time. The inset plot describes the relationship between mean whole tumour ADC for the 5-FC treated (filled symbols) and saline (open symbols) treated groups. The horizontal bar indicates the duration of drug or vehicle administration. Asterisks indicate statistically significant differences ($P < 0.02$) between treated and control groups.

space). Voxels from the entire tumour mass were summed together and plotted in a histogram format (Fig. 6 upper right). While this format removes spatial information as related to anatomical position, it allows the display of all of the values obtained from the entire tumour in a single plot providing for visualisation of the changes over time. Diffusion histograms plotted for this rat at days 21, 24 and 26 postcell implantation remained essentially unchanged in ADC units except that they increased in area due to increased tumour volume. In contrast, a rat treated identically except that 5-FC was administered daily from day 18 through to day 28 yielded an entirely different effect on the diffusion MR image. The effects of 5-FC treatment on tumour diffusion are easily observed in Fig. 6 (lower left panel) as a heterogeneous distribution of bright voxels located throughout the tumour mass. The interpretation of these images is that the bright areas (high diffusion) represent regions of CD expression leading to conversion of 5-FC to the cytotoxic product, 5-FU, with subsequent cell death leading to regions of focal necrosis. Histogram analysis of this tumour over time is shown in Fig. 6 (lower right panel). In contrast to what was observed in the untreated animal (Fig. 6, upper right), the histogram for the 5-FC-treated animal broadened with a fraction of the histogram area moving to the right (higher diffusion) to an approximate mean of 1.5 ADC units. The fraction of tumour tissue that exhibited an increase in diffusion is interpreted as the relative fraction of the tumour that is undergoing a significant therapeutic response. The region of the histogram in the treated animal that did not increase but remained at approximately 1–1.2 ADC units is most likely reflective of the cell fraction which was not exposed to sufficient 5-FU concentrations. At day 28, administration of 5-FC was terminated and the tumour subsequently began to re-grow as shown by the day 34 histogram (Fig. 6, lower right). This histogram shows that re-population of the solid portion of the tumour was occurring with a corresponding loss of high–diffusion regions. This in fact was consistent with the observed recurrent tumour using anatomical MR images of the animal. Also reported was the fact that a diffusion MRI histogram obtained from a rat which succumbed early (e.g. day 25 postcell implantation) with that of a longer surviving animal (e.g. day 44) had striking differences in diffusion changes [13]. The animal which had a minimal improvement in overall survival was found to have a relatively minimal increase in overall tumour diffusion during the course of treatment. In contrast, an animal with a much longer life-span had a large increase in tumour diffusion values over a significant fraction of the overall tumour mass. This study indicated that the magnitude of change in tumour diffusion values may correlate with

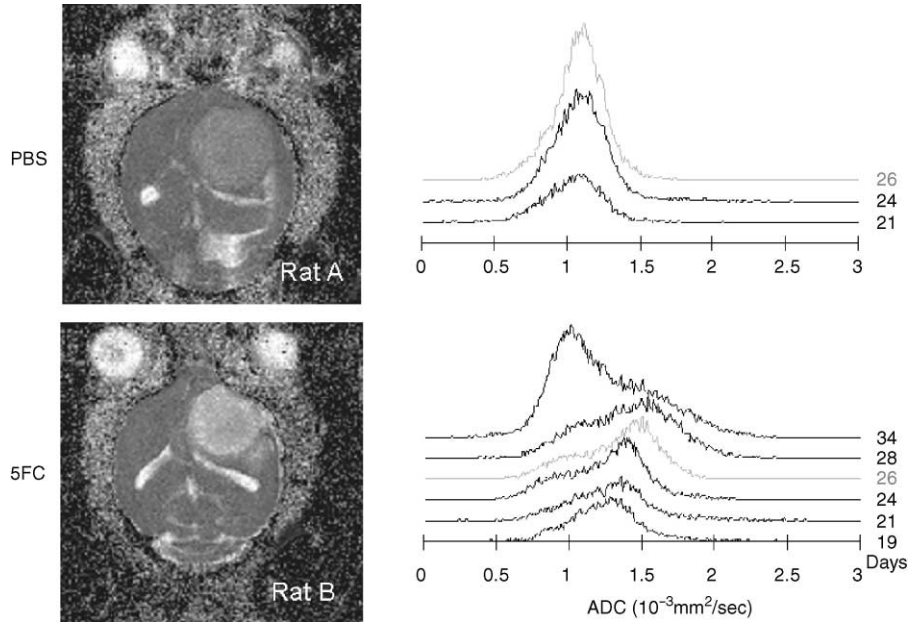

Fig. 6. Representative ADC maps of phosphate-buffered saline (PBS) control (top left) and 5-fluorocytosine (5-FC)-treated tumours (bottom left) at 7 days postinitiation of 5-FC administration. Note the areas of increased ADC (bright regions) within the 5-FC-treated tumour compared with control animal. Serial histograms of tumour pixel ADC values from the control (top right) and the 5-FC-treated animal (bottom right). The number of days post-initiation of 5-FC treatment is shown to the right of each histogram. Administration of the adenoviral vector did not affect the average tumour diffusion values as shown in the control. Treatment with 5-FC produced a non-uniform increase in tumour diffusion values which is interpreted to be due to heterogeneous expression of the CD transgene within the tumour mass due to the limitations of direct intratumoral injection of the vector.

therapeutic outcome [13]. Hence, diffusion MRI may provide an early, spatial indicator of animal tumour response in a wide variety of therapeutic paradigms.

4.2. Imaging of transgene expression

The use of non-invasive imaging technologies including radionuclide or optical reporters for evaluation and quantitation of transgene expression is an exciting area of research and the subject of review [15,19,20,22,39]. We have also recently reported that BLI can be used for repetitive measurements of transgene expression for assessing gene expression levels following adenoviral-mediated delivery of *yCD* [13]. These types of imaging applications provide kinetic information related to temporal changes associated with *in vivo* gene expression to be non-invasively probed over time. For example, BLI was used to monitor the longevity of cells which produced the cytotoxic product, 5-FU (e.g. 'factory' cells) following intratumoral administration of an adenoviral vector containing both the *yCD* and *luciferase* transgenes. Direct intratumoral injection of the *yCD* adenoviral vector was found to produce a heterogeneous distribution of yCD-positive cells within the 9L tumour mass. Assessment of the spatial distribution of yCD-expressing glioma cells was accomplished using immunohistochemical staining of 9L rat brain sections. Shown in Fig. 7a is a representative section of a rat brain tumour prepared 1 day following the second of two adenoviral injections as previously described in Ref. [13]. Expression of yCD was observed (brown coloured cells) within the tumour tissue and was found to be non-uniformly distributed within the tumour. BLI of this animal prior to sacrifice revealed the presence of a high level of luciferase activity (Fig. 7b). In contrast, a bioluminescence image acquired from a different animal at day 18 postinitiation of 5-FC treatment revealed very low levels of luciferase activity (Fig. 7d) which correlated with the near absence of CD immunohistochemistry from the tumour tissue (Fig. 7c) obtained from Rat #1. The ability to follow transgene expression levels will provide invaluable information related to the efficiency and kinetics of transgene expression which will greatly assist in, for example, the optimisation of prodrug dosing schedules. These types of surrogate markers for gene expression using BLI and correlation with spatial heterogeneity and magnitude of therapeutic response using diffusion MRI will ultimately facilitate preclinical optimisation of gene therapy paradigms prior to translation into the clinical setting.

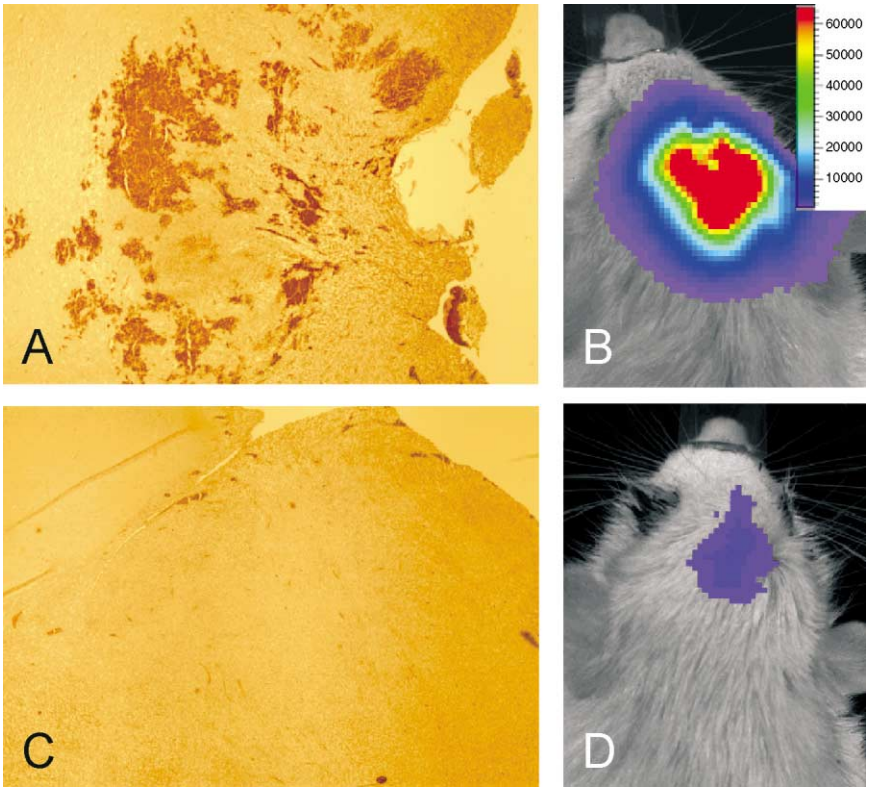

Fig. 7. (a) Representative CD immunohistochemical-stained section of a 9L tumour which was treated with CD adenovirus revealing significant, heterogeneous expression of CD within the tumour tissue. (b) Corresponding image of luciferase activity acquired using the BLI system which revealed significant photon emission indicating a high level of luciferase activity due to CD/Luc adenoviral injection/expression. (c) CD immunohistochemical-stained section of Rat # 1 (see Fig. 5) at day 18 posttreatment with 5-fluorocytosine (5-FC). Note the diminished expression of CD which also corresponded to limited detection of luciferase expression by BLI on day 18 as shown in Panel (d).

4.3. Non-invasive detection of transgene activity

While optical and radionuclide imaging modalities are useful for evaluating transgene expression levels in living organisms, it is not feasible to specifically monitor individual metabolites using these techniques. The use of fluorine-19 (^{19}F) magnetic resonance spectroscopy (MRS) for quantitatively evaluating the yCD-catalysed conversion of 5-FC to 5-FU has recently been reported [50]. This approach is viable since the prodrug used in this therapeutic paradigm contains a fluorine atom and is administered at concentrations which can be observed using *in vivo* ^{19}F MRS. In this study, mice with subcutaneous HT29 or HT29/yCD carcinomas were injected with 5-FC. The presence of 5-FC could be non-invasively detected in HT29 tumours as shown in the spectrum displayed in Fig. 8a. When tumours expressed yCD (HT29/yCD), enzymatic conversion of 5-FC to 5-FU could be observed dynamically over time with subsequent cellular conversion to additional metabolites (Fig. 8b). This approach is also quantitative since the area under the individual peaks can be converted to absolute metabolite concentration with appropriate calibration. This allowed for pharmacokinetic modelling of 5-FC conversion to 5-FU by endogeneous enzymes based upon the dynamic data provided by ^{19}F MRS. This yielded measurements of *yCD* gene expression levels and the rate of fluoronucleoside synthesis in individual animals [50].

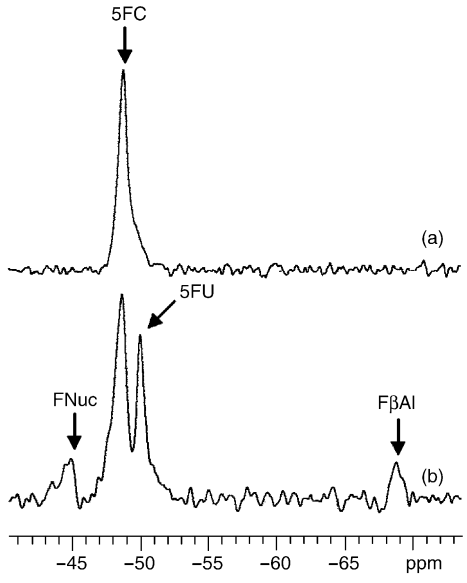

Fig. 8. (a) *In vivo* ^{19}F spectra of a subcutaneous tumour obtained 120–150 min after an intraperitoneal (i.p.) injection of 1 g/kg 5-fluorocytosine (5-FC). (a) Untransduced HT29 carcinoma and (b) HT29 carcinoma cells constituatively expressing yCD. Note that the yCD-expressing tumour cells were able to metabolise the prodrug into various metabolites as detected using magnetic resonance spectroscopy (MRS). ppm, parts per million.

5. Summary

Non-invasive imaging of anatomy coupled with improved imaging of function (biochemistry, physiology and cellularity) and molecular events will yield significant improvement in our understanding of the biology and pathophysiology of neoplastic diseases. The current imaging technologies and reporter genes for investigating gene expression and molecular events in living tissue are propelling the burgeoning field of molecular imaging rapidly forward into vitally important areas of research in biology and medicine. It is anticipated that molecular imaging will provide specific and complementary information which, when combined with anatomical imaging, will revolutionise our current applications of imaging in both drug discovery and clinical care.

Acknowledgements

This work was supported in part by the following research grants from the NIH/NCI: PO1CA85878, P20CA86442, and R24CA83099.

References

1. Weizsaecker M, Deen DF, Rosenblum ML, *et al.* The 9L rat brain tumor: description and application of an animal model. *J Neurol* 1981, **224**, 183–192.
2. Ross BD, Zhao YJ, Neal ER, *et al.* Contributions of cell kill and posttreatment tumor growth rates to the repopulation of intracerebral 9L tumors after chemotherapy: an MRI study. *Proc Natl Acad Sci USA* 1998, **95**, 7012–7017.
3. Hoffman JM. Imaging in cancer: a National Cancer Institute "extraordinary opportunity". *Neoplasia* 2000, **2**, 5–8.
4. Galons JP, Altbach MI, Paine-Murrieta GD, Taylor CW, Gillies RJ. Early increases in breast tumor xenograft water mobility in response to paclitaxel therapy detected by non-invasive diffusion magnetic resonance imaging. *Neoplasia* 1999, **1**, 13–117.
5. Gilead A, Neeman M. Dynamic remodeling of the vascular bed precedes tumor growth: MLS ovarian carcinoma spheroids implanted in nude mice. *Neoplasia* 1999, **1**, 226–230.
6. Bogdanov Jr. A, Marecos E, Cheng HC, *et al.* Treatment of experimental brain tumors with trombospondin-1 derived peptides: an in vivo imaging study. *Neoplasia* 1999, **1**, 438–445.
7. Evelhoch JL, Gillies RJ, Karczmar GS, *et al.* Applications of magnetic resonance in model systems: cancer therapeutics. *Neoplasia* 2000, **2**, 152–165.
8. Kurhanewicz J, Vigneron DB, Nelson SJ. Three-dimensional magnetic resonance spectroscopic imaging of brain and prostate cancer. *Neoplasia* 2000, **2**, 166–189.
9. Kaplan O, Firon M, Vivi A, Navon G, Tsarfaty I. HGF/SF activates glycolysis and oxidative phosphorylation in DA3 murine mammary cancer cells. *Neoplasia* 2000, **2**, 365–377.
10. Rehemtulla A, Stegman LD, Cardozo SJ, *et al.* Rapid and quantitative assessment of cancer treatment response using in vivo bioluminescence imaging. *Neoplasia* 2000, **2**, 491–495.
11. Fleige G, Nolte C, Synowitz M, *et al.* Magnetic labeling of activated microglia in experimental gliomas. *Neoplasia* 2001, **3**, 489–499.

12. Bogdanov A, Matuszewski L, Bremer C, Petrovsky A, Weissleder R. Oligomerization of paramagnetic substrates result in signal amplification and can be used for MR imaging of molecular targets. *Mol Imag* 2002, **1**, 16–23.
13. Rehemtulla A, Hall DE, Stegman LD, *et al*. Molecular imaging of gene expression and efficacy following adenoviral-mediated brain tumor gene therapy. *Mol Imag* 2002, **1**, 43–55.
14. Hogemann D, Josephson L, Weissleder R, Basilion JP. Improvement of MRI probes to allow efficient detection of gene expression. *Bioconjug Chem* 2000, **11**, 941–946.
15. Bremer C, Tung CH, Weissleder R. In vivo molecular target assessment of matrix metalloproteinase inhibition. *Nat Med* 2001, **7**, 743–748.
16. Gillies RJ, Bhujwalla ZM, Evelhoch J, *et al*. Applications of magnetic resonance in model systems: tumor biology and physiology. *Neoplasia* 2000, **2**, 139–151.
17. Bhujwalla ZM, Artemov D, Natarajan K, Ackerstaff E, Solaiyappan M. Vascular differences detected by MRI for metastatic versus nonmetastatic breast and prostate cancer xenografts. *Neoplasia* 2001, **3**, 143–153.
18. Pilatus U, Ackerstaff E, Artemov D, *et al*. Imaging prostate cancer invasion with multi-nuclear magnetic resonance methods: the Metabolic Boyden Chamber. *Neoplasia* 2000, **2**, 273–279.
19. Tjuvajev JG, Joshi A, Callegari J, *et al*. A general approach to the non-invasive imaging of transgenes using cis-linked herpes simplex virus thymidine kinase. *Neoplasia* 1999, **1**, 315–320.
20. Gambhir SS, Barrio JR, Phelps ME, *et al*. Imaging adenoviral-directed reporter gene expression in living animals with positron emission tomography. *Proc Natl Acad Sci USA* 1999, **96**, 2333–2338.
21. Mankoff DA, Dehdashti F, Shields AF. Characterizing tumors using metabolic imaging: PET imaging of cellular proliferation and steroid receptors. *Neoplasia* 2000, **2**, 71–88.
22. Gambhir SS, Herschman HR, Cherry SR, *et al*. Imaging transgene expression with radionuclide imaging technologies. *Neoplasia* 2000, **2**, 118–138.
23. Ponomarev V, Doubrovin M, Lyddane C, *et al*. Imaging TCR-dependent NFAT-mediated T-cell activation with positron emission tomography in vivo. *Neoplasia* 2001, **3**, 480–488.
24. Dyszlewski M, Blake HM, Dahlheimer JL, Pica CM, Piwnica-Worms D. Characterization of a novel 99mTc-carbonyl complex as a functional probe of MDR1 P-glycoprotein transport activity. *Mol Imag* 2002, **1**, 24–36.
25. Hackman T, Doubrovin M, Balatoni J, *et al*. Imaging expression of cytosine deaminase- herpes virus thymidine kinase fusion gene (CD/TK) expression with [124I]FIAU and PET. *Mol Imag* 2002, **1**, 36–42.
26. Hay RV, Cao B, Skinner RS, *et al*. Radioimmunoscintigraphy of tumors autocrine for human met and hepatocyte growth factor/scatter factor. *Mol Imag* 2002, **1**, 56–62.
27. Burt BM, Humm JL, Kooby DA, *et al*. Using positron emission tomography with [(18)F]FDG to predict tumor behavior in experimental colorectal cancer. *Neoplasia* 2001, **3**, 189–195.
28. Kristensen CA, Hamberg LM, Hunter GJ, *et al*. Changes in vascularization of human breast cancer xenografts responding to antiestrogen therapy. *Neoplasia* 1999, **1**, 518–525.
29. Paulus MJ, Gleason SS, Kennel SJ, Hunsicker PR, Johnson DK. High resolution X-ray computed tomography: an emerging tool for small animal cancer research. *Neoplasia* 2000, **2**, 62–70.
30. Jacobs A, Dubrovin M, Hewett J, *et al*. Functional coexpression of HSV-1 thymidine kinase and green fluorescent protein: implications for noninvasive imaging of transgene expression. *Neoplasia* 1999, **1**, 154–161.
31. Fujimoto JG, Pitris C, Boppart SA, Brezinski ME. Optical coherence tomography: an emerging technology for biomedical imaging and optical biopsy. *Neoplasia* 2000, **2**, 9–25.
32. Tromberg BJ, Shah N, Lanning R, *et al*. Non-invasive in vivo characterization of breast tumors using photon migration spectroscopy. *Neoplasia* 2000, **2**, 26–40.
33. Vajkoczy P, Ullrich A, Menger MD. Intravital fluorescence videomicroscopy to study tumor angiogenesis and microcirculation. *Neoplasia* 2000, **2**, 53–61.
34. Ramanujam N. Fluorescence spectroscopy of neoplastic and non-neoplastic tissues. *Neoplasia* 2000, **2**, 89–117.
35. Pedersen MW, Holm S, Lund EL, Hojgaard L, Kristjansen PE. Coregulation of glucose uptake and vascular endothelial growth factor (VEGF) in two small-cell lung cancer (SCLC) sublines in vivo and in vitro. *Neoplasia* 2001, **3**, 80–87.
36. Kragh M, Quistorff B, Lund EL, Kristjansen PE. Quantitative estimates of vascularity in solid tumors by non-invasive near-infrared spectroscopy. *Neoplasia* 2001, **3**, 324–330.
37. Vordermark D, Shibata T, Martin Brown J. Green fluorescent protein is a suitable reporter of tumor hypoxia despite an oxygen requirement for chromophore formation. *Neoplasia* 2001, **3**, 527–534.
38. Edinger M, Sweeney TJ, Tucker AA, *et al*. Noninvasive assessment of tumor cell proliferation in animal models. *Neoplasia* 1999, **1**, 303–310.
39. Contag CH, Jenkins D, Contag PR, Negrin RS. Use of reporter genes for optical measurements of neoplastic disease in vivo. *Neoplasia* 2000, **2**, 41–52.
40. Padera TP, Stoll BR, So PTC, Jain RK. Conventional and high-speed intravital multiphoton laser scanning microscopy of microvasculature, lymphatics, and leukocyte-endothelial interactions. *Mol Imag* 2002, **1**, 9–15.
41. Sameni M, Moin K, Sloane BF. Imaging proteolysis by living human breast cancer cells. *Neoplasia* 2000, **2**, 496–504.
42. Hawrysz DJ, Sevick-Muraca EM. Developments toward diagnostic breast cancer imaging using near-infrared optical measurements and fluorescent contrast agents. *Neoplasia* 2000, **2**, 388–417.
43. Stejskal EO, Tanner J. Spin diffusion measurements: spin-echoes in the presence of a time-dependent field gradient. *J Chem Phys* 1965, **42**, 288–292.
44. Ross BD, Chenevert TL, Kim B, Ben-Yoseph O. Magnetic resonance imaging and spectroscopy: application to experimental neuro-oncology. *Q Magn Reson Biol Med* 1994, **1**, 89–106.
45. Zhao M, Pipe JG, Bonnett J, Evelhoch JL. Early detection of treatment response by diffusion-weighted 1H-NMR spectroscopy in a murine tumour in vivo. *Br J Cancer* 1996, **73**, 61–64.
46. Chenevert TL, McKeever PE, Ross BD. Monitoring early response of experimental brain tumors to therapy using diffusion magnetic resonance imaging. *Clin Cancer Res* 1997, **3**, 1457–1466.
47. Ross BD, Ben-Yoseph O, Chenevert TL. In vivo magnetic resonance imaging and spectroscopy: application to brain tumors. *Magn Reson Spec Imag Nurochem* 1997, **8**, 145–178.
48. Stegman LD, Rehemtulla A, Hamstra DA, *et al*. Diffusion MRI detects early events in the response of a glioma model to the yeast cytosine deaminase gene therapy strategy. *Gene Ther* 2000, **7**, 1005–1010.
49. Chenevert TL, Stegman LD, Taylor JM, *et al*. Diffusion magnetic resonance imaging: an early surrogate marker of therapeutic efficacy in brain tumors. *J Natl Cancer Inst* 2000, **92**, 2029–2036.
50. Stegman LD, Rehemtulla A, Beattie B, *et al*. Noninvasive quantitation of cytosine deaminase transgene expression in human tumor xenografts with in vivo magnetic resonance spectroscopy. *Proc Natl Acad SciUSA* 1999, **96**, 9821–9826.